Chemical Engineering Journal 349 (2018) 428–437

Contents lists available at ScienceDirect

Chemical Engineering Journal

journal homepage: www.elsevier.com/locate/cej

Pore-scale study of effects of macroscopic pores and their distributions on reactive transport in hierarchical porous media

Li Chen[a,*], Ruiyuan Zhang[a], Ting Min[b], Qinjun Kang[c], Wenquan Tao[a]

[a] Key Laboratory of Thermo-Fluid Science and Engineering of MOE, School of Energy and Power Engineering, Xi'an Jiaotong University, Xi'an, Shaanxi 710049, China
[b] State Key Laboratory for Mechanical Behavior of Materials, School of Materials Science and Engineering, Xi'an Jiaotong University, 28 Xianning West Road, Xi'an, Shaanxi Province 710049, China
[c] Computational Earth Science, EES-16, Earth and Environmental Sciences Division, Los Alamos National Laboratory, Los Alamos, NM 87544, USA

HIGHLIGHTS

- Pore-scale reactive transport in hierarchical porous media is studied.
- Macroscopic pores in micro/meso porous media can enhance mass transport.
- Opposite effects of adding macropores for reaction rate are revealed.
- Effects of gradient distribution of macropores are explored.
- Optimized structures of hierarchical porous media are proposed.

ARTICLE INFO

Keywords:
Hierarchical porous media
Pore-scale
Gradient distribution
Lattice Boltzmann method
Catalyst utilization

ABSTRACT

For applications of reactive transport in porous media, optimal porous structures should possess both high surface area for reactive sites loading and low mass transport resistance. Hierarchical porous media with a combination of pores at different scales are designed for this purpose. Using the lattice Boltzmann method, pore-scale numerical studies are conducted to investigate diffusion-reaction processes in 2D hierarchical porous media generated by self-developed reconstruction scheme. Complex interactions between porous structures and reactive transport are revealed under different conditions. Simulation results show that adding macropores can greatly enhance the mass transport, but at the same time reduce the reactive surface, leading to complex change trend of the total reaction rate. Effects of gradient distribution of macropores within the porous medium are also investigated. It is found that a front-loose, back-tight (FLBT) hierarchical structure is desirable for enhancing mass transport, increasing total reaction rate, and improving catalyst utilization. On the whole, from the viewpoint of reducing cost and improving material performance, hierarchical porous structures, especially gradient structures with the size of macropores gradually decreasing along the transport direction, are desirable for catalyst application.

1. Introduction

Reactive transport in porous media is widely encountered in scientific problems and engineering applications. Typical examples include fuel cells [1,2], flow batteries [3,4], and thermochemical energy storage [5,6]. To enhance the reactive transport, porous media with high surface area (SA) have been widely adopted because a high SA results in more active sites, which is favorable for surface-related process such as adsorption and catalysis. Much effort thus has been devoted to the development of porous media with high SA. Since SA increases as the solid particle size decreases at a fixed volume fraction, porous media with high SA usually possess the characteristic of nanoscale solid particles and pores. For example, in catalyst layers (CLs) of proton exchange membrane fuel cells (PEMFCs), carbon black (Vulcan XC-72, VC) is the most common support of catalysts (typically platinum particles). The typical size of carbon black particle is about 20–40 nm, and aggregation of these carbon particles during electrode fabrication leads to abundant nanoscale pores between these primary particles [7].

For reactive transport in porous media, besides active sites, another important aspect is the mass transport capacity of the porous media [8]. Of course, even if a porous medium has a high SA and provides

* Corresponding author.
E-mail address: lichennht08@mail.xjtu.edu.cn (L. Chen).

https://doi.org/10.1016/j.cej.2018.05.106
Received 13 March 2018; Received in revised form 16 May 2018; Accepted 18 May 2018
Available online 19 May 2018
1385-8947/

sufficient reaction sites, if these active sites are not available to the reactant due to high mass transport resistance, the reactive transport will not be as effective as desired during practical applications. Unfortunately, in a porous medium with a dominant pore size of a few to tens of nanometers, the gas transfer is poor as around normal pressure and temperature the dominant transport mechanism is Knudsen diffusion which is extremely slow [9]. Therefore, it is highly desirable to enhance mass transport in such nanoscale porous media to improve their performance.

To improve mass transport in nanoscale porous media, the utilization of hierarchical porous structures is an area of growing interest [10]. In such hierarchical porous structures, pores at multiple length scales are combined to achieve multi-objective optimization. According to the pore-size terminology proposed by International Union of Pure and Applied Chemistry (IUPAC) [11], pores can be classified into micropores (< 2 nm), mesopores (2–50 nm) and macropores (> 50 nm), and in this study this terminology is followed. In a hierarchical porous medium with multimodal pore size distribution (PSD), micropores and small mesopores result in a high SA and thus a large number of active sites, while large mesopores and macropores facilitate the mass transport and thus guarantee the accessibility of the active sites to the reactants. Such hierarchical porous media have been proven to improve the material performance. To name only a few, Fang et al. [12] fabricated ordered hierarchical nanostructured carbon which has high SA for dispersion of small Pt particles and well-connected mesopores (around 20 nm) as well as macropores (around 440 nm) for mass transport, resulting in 53–88% increase of the maximum power density compared with traditional VC-supported Pt. Song et al. [13] found that in fuel cell ordered mesoporous carbon exhibits superior reaction activity than disordered wormhole-like mesoporous carbon, even if the pore size distributions of the two carbon materials are similar. It is mainly because the former one has the high ordered degree and very good 3D interconnection of mesopores, leading to better mass transport, and thus Pt particles can be more easily accessed by the electrolyte. Proietti et al. [14] found that an over-twofold increase in current density of a PEMFC is mainly caused by the improved mass transport due to numerous pores of about 50 nm in their Iron-based cathode catalysts. Liang et al. [15] developed hierarchical porous carbons with ultramicropore, micropore and mesopore centred at 0.6, 1.4 and 12 nm, respectively, and it was found that the hierarchically porous carbons show very high oxygen reduction reaction activity. In conclusion, such hierarchical porous media have been fabricated and proved to improve performance of several applications including adsorption, energy conversion, and energy storage, and one can refer to recent reviews for more details [16–18].

From the above, it can be seen that porous structure and morphology play critical roles on the reactive transport process in hierarchical porous media. Therefore, a deep understanding of the reactive transport phenomena and the strong interaction between transport processes and the porous structures is thus required for delicately fabricating the hierarchical porous media. For current experimental techniques, studying these processes occurring at the nanoscale is still challenging. Pore-scale modeling is a powerful and efficient way for this purpose. Unlike continuum-scale modeling making homogeneous assumption of porous media and thus requiring empirical and constitutive relationships for determining macroscopic transport properties, pore-scale modeling accounts for realistic structures of a porous medium and solves physics-based governing equations in the porous structures, leading to detailed distributions of important variables (velocity, concentration, temperature, reaction rate, etc.). Thus, pore-scale modeling has been widely adopted to investigate multiple physicochemical processes in porous media, to explore interaction between transport processes and porous structures, and to provide optimization of structures and topologies of porous media. Different numerical methods including top-down approaches such as traditional finite-type methods (FVM, FEM and FDM) and bottom-up approaches such as the lattice Boltzmann method (LBM) and the molecular dynamics (MD). It is worth mentioning that the pore-network (PN) modeling also has been widely adopted for transport in porous media [19]. However, PN modeling is a rule-based model, in which topologically and geometrically idealized porous structures consisting of pores connected by throats are adopted rather than the realistic structures of porous media. Besides, in pores and throats of PN modeling, simplified hydrodynamic and reactive equations are solved such as cubic law for flow. Thus, PN modeling actually simulates porous media at a scale between pore-scale modeling and continuum-scale modeling. Although it has played an important role in revealing physics of flow in porous media, it is not suitable for the task of optimizing pore structures.

Among the numerical methods adopted for pore-scale simulation, the lattice Boltzmann method (LBM) has an advantage to treat complex boundaries due to its kinetic nature and thus is particularly suitable for modeling transport processes in porous media [20,21]. The LBM has been widely adopted in the literature for reactive transport processes in porous media [22,23]. It was adopted to study convective mass transfer with surface reaction in fixed-bed reactors [24]. It was later improved to simulate large *Pe* number (relative strength between fluid flow and diffusion) mass transport process in ordered and disordered porous media [25]. By distinguishing primary and secondary species in multicomponent system, a LB pore-scale model [26] was proposed for multicomponent reactive transport process in porous media with both homogeneous and heterogeneous reactions considered, greatly reducing the computational costs. A LB pore-scale model considering Stefan–Maxwell diffusion process was also developed and applied to solid oxide fuel cell (SOFC) porous anode [27]. Further considering the coupling between mass transport and charge transfer, the LBM was applied to electrochemical reaction process in SOFC porous anode obtained by focused ion beam scanning electron microscopy (FIB-SEM) [28], and over-potential and detailed current density distributions inside the porous anode were obtained. It was also adopted to study dynamic adsorption process in a crenelated pore representing hierarchical porous media [29], taking into account the balance between adsorption and desorption. A reactive transport LB model, which takes into account the effects of pores inside the solid matrix within one pixel (one computational mesh), was developed by Tian and Wang [30,31]. Based on 3D porous morphology generated by CT scan, this model was employed to study reactive transport and solid dissolution related to CO_2 sequestration. The LBM is also a major tool for investigating pore-scale phenomena in porous electrodes of PEMFCs [22] such as fluid flow, mass transport, multiphase flow and reactive transport [32–34]. A major drawback of LB pore-scale study is the relatively high computational resources required, thus there are also attempts to develop multiscale simulation strategy by coupling the LBM and continuum-scale models for physicochemical processes in porous media [35].

From the above review, it can be concluded that adopting hierarchical structures has been demonstrated to facilitate reactive transport in porous media. However, there are few studies regarding optimization of the pore size and topology of the hierarchical porous media for a chosen application [29]. This is largely due to the fact that it remains challenging for the state-of-the-art techniques to fabricate delicately designed morphologies of porous media, for example, hierarchical porous media with specific size of macroscopic and microscopic pores. Pore-scale numerical studies can lead the effort and provide guidance for fabrication of better hierarchical structures. Of course, a deep understanding of the physicochemical phenomena in hierarchical porous media is crucial for optimizing existing materials as well as designing new ones. Therefore in the present study, the LBM is adopted to study several open fundamental questions related to reactive transport in hierarchical structures including reactive transport processes in interconnected micro, meso and macro-pores, the coupling mechanisms between hierarchical structures and reactive transport, and the influence of large mesopores and macropores as well as topologies on material performance and catalyst utilization. The rest of the present

study is arranged as follows. In Section 2, the porous structures under investigation are introduced. Then in Section 3, the LB pore-scale model for reactive transport in porous media is presented. In Section 4, simulation results of reactive transport in hierarchical porous media and effects of pore size and topology on material performance are discussed in detail. Finally, a conclusion is drawn in Section 5.

2. Porous structure generation

The porous structures studied in this study are generated by a self-developed code. The general scheme to reconstruct the porous medium is to randomly place circular solid particles into the computational domain, as described as follows: Step 1: the first solid circle is generated in the computational domain. Random number generators are employed to determine its center (i,j) and diameter d; Step 2: random number generators are used to generate the center and diameter of a trial circle. Further, a random number generator is employed to determine whether or not the next circle is allowed to overlap with existing circles in the computational domain. a) If the circle is required to overlap with existing circles, it must overlap with at least one existing circle and the overlapping portion should not be greater than the overlap tolerance ξ. Here, ξ, defined as the ratio between the area of the overlapping region of a circle with other circles and its total area, determines the maximum overlapping area (volume in 3D); b) If overlapping is not allowed, the new circle must not touch any existing circles, and a minimum distance δ between trial circle and existing circles should be satisfied; Step 3: Repeat Step 2.

The diameter of circles follows a uniform distribution ($< d >$ - 12 nm, $< d >$ +12 nm), with $< d >$ the mean diameter chosen as 20 nm (or 10 lattices in the simulation for size of one lattice as 2 nm). The overlapping probability p_0 is set as 0.001, indicating a low probability for solid particle overlapping. ξ is set as 0.5 and δ is set as 10 nm. As the above generation procedure proceeds, the total area of the solid circles increases. Thus, it becomes increasingly harder to add a new circle in the later stage, as the center and diameter of a trial circle are randomly generated. For example, it is found that when the porosity reaches 0.65 (as shown in Fig. 1(a)), more than 200 trials are required to add a new circle in a 2000 × 400 lattice domain.

An improved algorithm based on PSD is proposed to enhance the reconstruction efficiency. The further steps continued from Steps 1–3 are implemented as follows: Step 4: PSD is determined using the skeletization method [36]. In this method, the local pore size of any void node P is defined as the radius of the largest circle which is centered inside the void space and includes point P. The largest local circle is centered at point O with radius r (Fig. 1(b)); Step 5: the void node with the largest pore size r_{max} is selected to add a new circle with radius as r_{max}-5. Here 5 lattices are subtracted due to the minimum distance δ; Step 6: repeat Steps 4 and 5 until r_{max} is less than 8 lattices.

Fig. 1(d) shows the final porous structure generated by further implementing Steps 4–6, with final porosity of 0.515. It can be observed that at the domain scale solid circles with different sizes are quite uniformly distributed. Fig. 1(c) shows the PSD of the structures in Fig. 1(d), with a peak value of diameter as 14 nm. The minimum pore size is 10 nm, consistent with minimum distance δ. Due to the restriction of δ, the gap between circles are sufficient to guarantee LB mass transport simulations. All the pores are with size in the range of 2–50 nm, and thus are mesopores according to IUPAC [11]. Further, hierarchical porous media are generated by putting large mesopores and macropores in the original porous medium shown in Fig. 1(d). The details of the hierarchical porous structures together with the reactive transport processes will be discussed in Section 4. Besides, hierarchical porous structures with gradient distributions of the large mesopores and macropores are also discussed in Section 4.

3. Physicochemical processes and numerical method

3.1. Physicochemical processes

To clearly illustrate effects of porous structures and topologies on reactive transport in porous media, without loss of generality, diffusion-reaction processes in the generated porous structures are studied. In practical applications, fluid flow in such nanosize porous media usually is extremely weak and thus is not considered here. Reactant diffuses into the porous medium from left inlet. The governing equation for reactant concentration can be expressed as

$$\nabla\left(\left[\frac{1}{D_B}+\frac{1}{D_{Kn}}\right]^{-1}\nabla C\right)=0 \tag{1}$$

with D_B and D_{Kn} representing binary and Knudsen diffusion coefficients, respectively. D_{Kn} is calculated by

$$D_{Kn}=\frac{d_p}{3}\sqrt{\frac{8RT}{\pi M}} \tag{2}$$

d_p of each void node is determined by the PSD obtained from the skeletization method as discussed in Section 2. Thus, diffusivity of each void node is different for different local pore size.

On the solid surface, a first-order reaction takes place

$$D\frac{\partial C}{\partial \mathbf{n}}=kC \tag{3}$$

with k the reaction rate constant. Although seemingly simple, the reaction described by Eq. (3) can represent some complicated chemical reactions under some scenarios. For example, electrochemical reaction in PEMFC is described by the Butler-Volmer equation which relates the reaction flux to the local gas concentration and overpotential [37]. Effects of parameters in the Butler-Volmer equation such as exchange current density, reference oxygen concentration, transfer coefficient and overpotential can be lumped together into the reaction rate constant k, as widely adopted in the agglomerate model for reactive transport in catalyst layers of PEMFC [37].

3.2. Numerical method

In this work, the LBM is adopted to simulate both reaction and mass transport in the generated porous structures. The evolution equation for the concentration distribution function is as follows

$$g_i(\mathbf{x}+\mathbf{c}_i\Delta t,t+\Delta t)-g_i(\mathbf{x},t)=-\frac{1}{\tau_g}(g_i(\mathbf{x},t)-g_i^{eq}(\mathbf{x},t)) \tag{4}$$

where g_i is the concentration distribution function with velocity c_i at the lattice site $\mathbf{x}$ and time t. For mass transport, a D2Q5 (2 dimensional 5 lattice directions) lattice model is sufficient to accurately predict the diffusion process and properties, which can greatly reduce the computational resources compared with D2Q9 lattice model [35,38]. The velocities in D2Q5 lattice model are as follows

$$\mathbf{c}_i=\begin{cases}0 & i=0\\ (\pm1,0),(0,\pm1) & i=1\sim4\end{cases} \tag{5}$$

An equilibrium distribution g^{eq} that is linear in $\mathbf{u}$ is adopted

$$g_i^{eq}=C\left[J_i+\frac{1}{2}\mathbf{e}_i\cdot\mathbf{u}\right] \tag{6}$$

with J_i given by

$$J_i=\begin{cases}J_0 & i=0\\ (1-J_0)/4 & i=1,2,3,4\end{cases} \tag{7}$$

where the rest fraction J_0 can be selected from 0 to 1. The equilibrium distribution function given by Eq. (7) can cover a wide range of diffusivity by adjusting J_0, which is a prominent advantage of such an

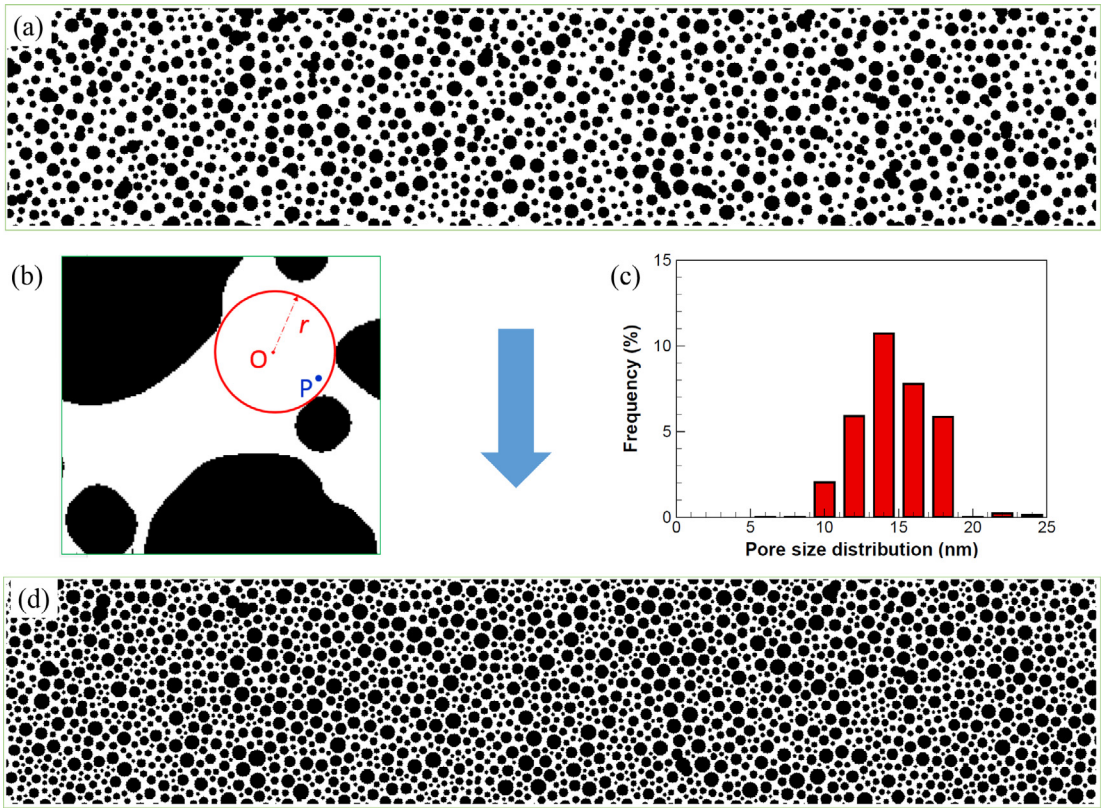

Fig. 1. Porous structure generation. (a) 2D porous medium with porosity of 0.65. (b) Schematic of skeletization method to determine local pore size. (c) Pore size distribution of final porous structures in (d) the final 2D porous medium generated with size of 2000 × 400 lattices and porosity of 0.515.

equilibrium distribution [38]. The accuracy and efficiency of the reduced D2Q5 model has been confirmed in other studies [33].The concentration is obtained by summation of distribution function $C = \sum g_i$. The relationship between diffusivity and relaxation time is as follows

$$D = \frac{1}{2}(1-J_0)(\tau_\varphi - 0.5) \tag{8}$$

As discussed in Section 2, diffusivity for each void node is different for different local pore size, thus the different relaxation time τ changes according to local diffusivity. Eqs. (4)–(6) can be proved to recover Eq. (1) using the Chapman–Enskog expansion [35].

Unlike conventional numerical methods where the fundamental variables are macro physical quantities (density, velocity, temperature and concentration, etc.), in the LB framework, the fundamental variables are the distribution functions. Therefore, boundary conditions based on the distribution functions are required when performing LB simulations. For reactive transport processes in this study, four types of boundary conditions are used: the concentration boundary condition for the inlet, the fully developed condition for the outlet, the periodic boundary condition for the top and bottom boundaries, and the reaction boundary condition described by Eq. (3) on solid surface. In the LB framework, for the concentration boundary condition, when the D2Q5 lattice model is used only one distribution function is not known and is obtained by subtracting the concentration from the other four known distribution functions. For the fully developed boundary condition, the unknown distribution function is simply set as the distribution function at the same direction of the neighboring void node. For periodic boundary condition, the outgoing distribution functions from the top boundary reenter the domain from the bottom boundary, and vice versa. Finally, for the reactive boundary condition described by Eq. (3), the boundary condition proposed in our previous work is employed [39], which can guarantee the mass conservation. The LB boundary condition is briefly introduced as follows. Suppose a flat wall along x direction, below and above which are solid and fluid regions, respectively. After each streaming step, g_2 is unknown and g_4 is known, and g_1 and g_3 do not affect the fluid domain and hence are not needed to calculate their values. The first-order moment of the distribution functions is [39]

$$\sum g_i \mathbf{e}_i = g_2 - g_4 = -D\nabla C = -kC \tag{9}$$

Further, the non-equilibrium portion of the distribution functions in opposite directions takes the opposite sign for a static wall, thus the following equation can be obtained

$$g_2 + g_4 = (g_2^{eq} + g_2^{neq}) + (g_4^{eq} + g_4^{neq}) = g_2^{eq} + g_4^{eq} \tag{10}$$

Combining Eqs. (9) and (10), the two unknown variables, concentration C on the solid surface and distribution function g_2 can be obtained.

4. Results and discussion

Self-developed LB code based on the numerical method introduced in Section 3 is adopted to simulate reactive transport processes in a 1000 × 400 subdomain of the porous structures shown in Fig. 1(d). The LB code is parallelized based on domain decomposition using Message Passing Interface (MPI). The entire domain is divided into 10 and 2 in the x and y, respectively, leading to 20 CPU cores used. For the lowest reaction rate constant k (1.0×10^{-7}) studied, the time required for reaching steady state is about 48 h, while for the highest k (1.0×10^{-3}), only 10 min are enough for simulation convergence.

4.1. Reactive transport in the original porous medium

Fig. 2 shows the concentration distribution in the original porous structures under different reaction rate constant k. As k increases from 1.0×10^{-7} to 1.0×10^{-3} in lattice units (or 1.91×10^{-3} to

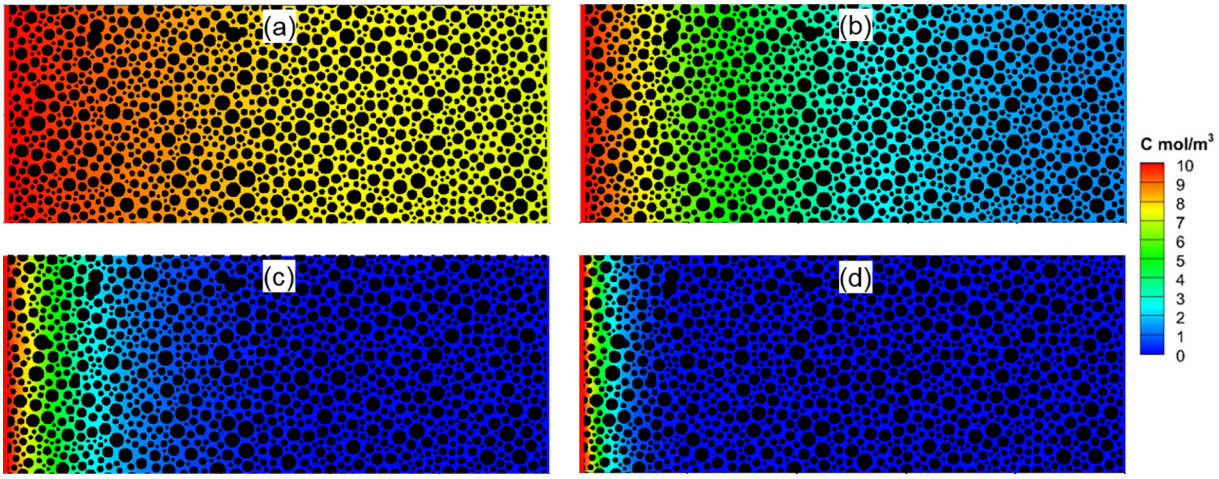

Fig. 2. Concentration distribution for the original porous structures under different reaction rate constant k: (a) 1.0×10^{-7}, (b) 1.0×10^{-6}, (c) 1.0×10^{-5} and (d) 1.0×10^{-3}.

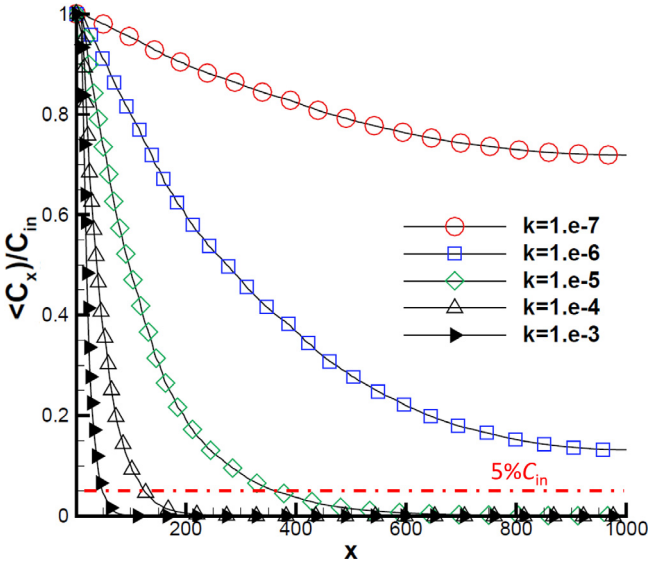

Fig. 3. The distribution of averaged reactant concentration along x direction in original porous medium under different reaction rate constant.

$1.91\ \mathrm{m\,s^{-1}}$ in physical units with $dx = 2.0 \times 10^{-9}$ m and $dt = 1.04 \times 10^{-14}$ s), more and more reactants are consumed near the left inlet. For $k = 1.0 \times 10^{-7}$, all the domain is full of reactant, while for $k = 1.0 \times 10^{-5}$ most of the domain is starved of reactant. Fig. 3 further shows the distribution of averaged reactant concentration along x direction. Note that showing in y axis is normalized value by inlet concentration C_{in}. It can be seen that under a higher k, reaction depth, which is defined as 95% penetration of the concentration, is lower. For example, for $k = 1.0 \times 10^{-3}$, the reaction depth is only about 50 lattices, much lower than the domain length 2000 nm. Thus most of the catalyst in the porous media is not utilized, causing a waste of the catalysts. Under such scenario, mass transport is the limiting factor for the reactive transport process, and it should be enhanced.

4.2. Effects of macropores

In nanoscale porous media such as that shown in Fig. 2, gas diffusion process around normal temperature and pressure is dominated by Knudsen diffusion mechanism due to the nanosize pores. It is well known that mass transport by Knudsen diffusion is very slow, which thus is required to be improved. Large mesopores and macropores are usually added in the domain for this purpose. Pore-scale studies are conducted in this section to investigate the effects of large pores. As shown in Fig. 4, macropores with square shape are added in the original porous structures leading to hierarchical porous structures. For all hierarchical structures studied, the number of large pores as well as the center of each large pore are the same. The only difference is the side length of the large pores. Thus the higher the side length, the bigger the macropores, and thus the higher the porosity of the hierarchical porous structures. In this study, uniform distributions of these large pores are adopted to avoid uncertainty caused by random distributions. In practice, it is usually observed that large pores are randomly distributed in the porous materials. Of course random distribution of large pores can be used in the simulations, but for each case, several structures should be generated with the same constraint parameters, and the results of these structures should be averaged to increase the result reliability. For more details of such random generation, one can refer to our previous studies [40]. It is worth mentioning that recently there have been several techniques proposed for fabricating ordered hierarchical porous media [17].

Fig. 4 shows the concentration distribution in the domain for two hierarchical structures, with side length of the large pores as 40 and 60 lattices (or 80 nm and 120 nm), respectively. Thus the pores added for the two structures belong to macropores. k is the same for both cases as

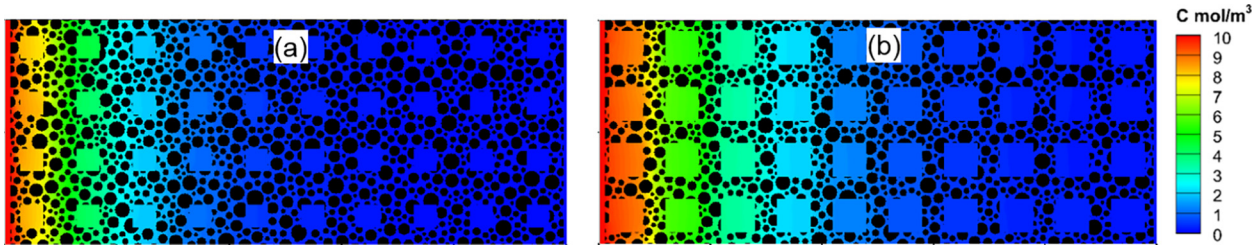

Fig. 4. Concentration distribution for two hierarchical porous structures, with side length of macropores as 40 and 60 lattices, respectively.

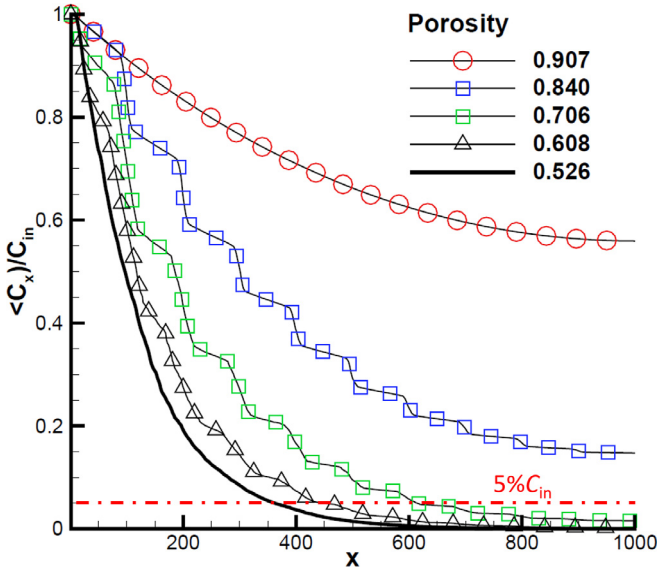

Fig. 5. The distribution of averaged reactant concentration along x direction in hierarchical porous structures with reaction rate constant $k = 1.0 \times 10^{-5}$.

1.0×10^{-5}. Compared Fig. 4 with Fig. 2(c), it can be observed that large pores play an role as fast pathways for mass transport, and thus the mass transport is greatly enhanced. This is confirmed by Fig. 5 where the average concentration along x direction is plotted for reaction rate constant $k = 1.0 \times 10^{-5}$. For the original structure with porosity = 0.526, the penetration depth is only about 360 lattices. With large pores added, the total porosity is increased, and the penetration depth is longer. For porosity as 0.608 and 0.706 (the corresponding side length of larges are 40 and 60 lattices, respectively), the penetration depth is about 450 and 640 lattices, respectively. For porosity further increased to 0.840 and 0.907 (side length of large pores as are 72 and 80 lattices, respectively), the entire domain is penetrated, indicating remarkable enhancement of mass transport.

Shown in Fig. 6 is the averaged reaction rate $< kC >$ on the catalyst surface against the reaction rate constant for different porosity values. The operator $< >$ is averaging operator, and $< kC >$ is obtained by summation of kC at each reaction site and then averaged by the number

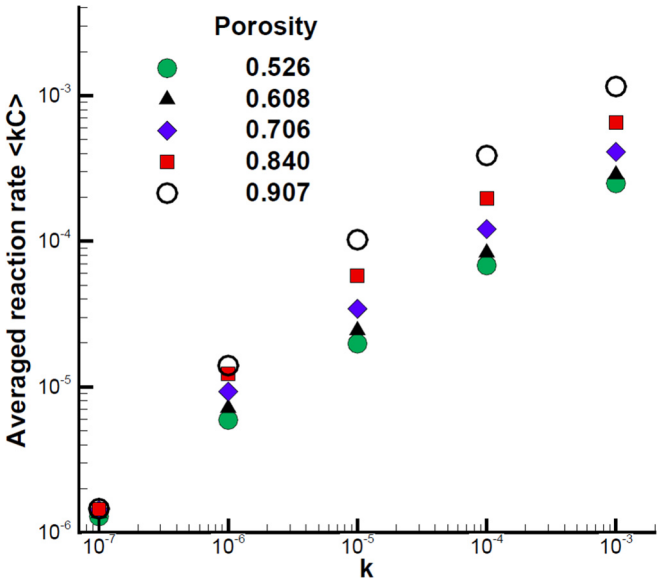

Fig. 6. Averaged reaction rate $< kC >$ on the solid surface as a function of reaction rate constant for different porous structures.

of the reaction sites. When the reaction rate constant k is relatively small ($k = 1.0 \times 10^{-7}$), mass transport is fast compared to reaction, and thus $< kC >$ for porous structures with different porosity is almost the same, indicating adding macropores has minimal effect on improving mass transport. As k increases, chemical reaction becomes faster, and it becomes more difficult for the reactant to penetrate the porous media. When k is relatively high (such as $k = 1.0 \times 10^{-5}$), the difference between different porosities is obvious. The higher the porosity, the faster the mass transport, leading to a higher $< kC >$. From the above discussion related to Figs. 4–6, it can be concluded that mass transport can be enhanced by macropores, especially at relatively high reaction rate constant. Now attention is turned to the total reaction rate $\psi = \sum kC$ in the catalyst, which is the summation of kC over all reaction sites. It can be adopted to evaluate the catalyst performance, such as amount of reactant converted, or the current density generated in PEMFC. Fig. 7 shows the variations of the total reaction rate under different porosity and reaction rate constant values. It is interesting to find that the change trends of total reaction rate under different reaction rate constant values are quite different from each other. In Fig. 7(a) with $k = 1.0 \times 10^{-7}$, the total reaction rate ψ monotonously decreases as porosity increases (or the side length of macropores increases); in Fig. 7(b) with $k = 1.0 \times 10^{-6}$, ψ firstly increases and then drops, showing a peak value; and in Fig. 7(c) and (d), ψ monotonously increases. Thus, although macropores can enhance mass transport in the porous media as demonstrated above, their effects on the total reaction rate are complex and are explained as follows.

In this study, the way to add macropores enhances mass transport (positive effect for reactive transport), but also reduces total surface area (negative effect). Under a relatively low reaction rate constant, the reactive transport inside porous media is limited by slow reaction, which is usually called reaction-controlled transport process. This means mass transport is sufficiently strong, and thus adding macropores has minimal effect on enhancing mass transport. In this scenario, the negative effect of large pores (i.e., the surface area reduction) outweighs their positive effect (i.e. mass transport enhancement), leading to a decrease of the total reaction rate as shown in Fig. 7(a). At moderate reactive rate constant, the mass transport within the porous media is relatively slow, as can be seen from Figs. 2 and 3 that the concentration for $k = 1.0 \times 10^{-6}$ significantly declines compared with that for $k = 1.0 \times 10^{-7}$. Under a low porosity, the positive effect of adding macropores outweighs the negative effect, and thus the total reaction rate first increases in Fig. 7(b) (before porosity = 0.706). However, as the porosity gets higher, the loss of reactive surface area cannot be compensated by the enhancement of mass transport, causing the total reaction rate to decline (after porosity = 0.706). Finally under relatively high reaction rate constant, mass transport becomes the limiting factor for the reactive transport, leading to transport-controlled processes. It can be seen from Figs. 2 and 3 that the reactant is totally consumed in a local region near the inlet and most of the region is not accessible to the reactant. In this case, adding macropores can significantly enhance the mass transport. Therefore, the total reaction rate monotonously increases as more large pores are added, as shown in Fig. 7(c) and (d). In conclusion, the diverse changing trends of total reaction rate under different reaction rate constants are a result of the competition between mass transport enhancement and reactive surface area reduction caused by adding macropores. Such complex trend also has been found in a recent pore-network modeling [41].

4.3. Effects of gradient distribution of macropores

In this section, macropores with different pore size are directionally placed inside the catalyst to study the effects of gradient distribution of macropores on the reactive transport processes. Usually, the porous media provide pathways for multiple reactants. For example, catalyst layer of PEMFCs provides pathway not only for gas in pores, but also for electrons in solid and for protons in electrolyte. Therefore, the catalyst

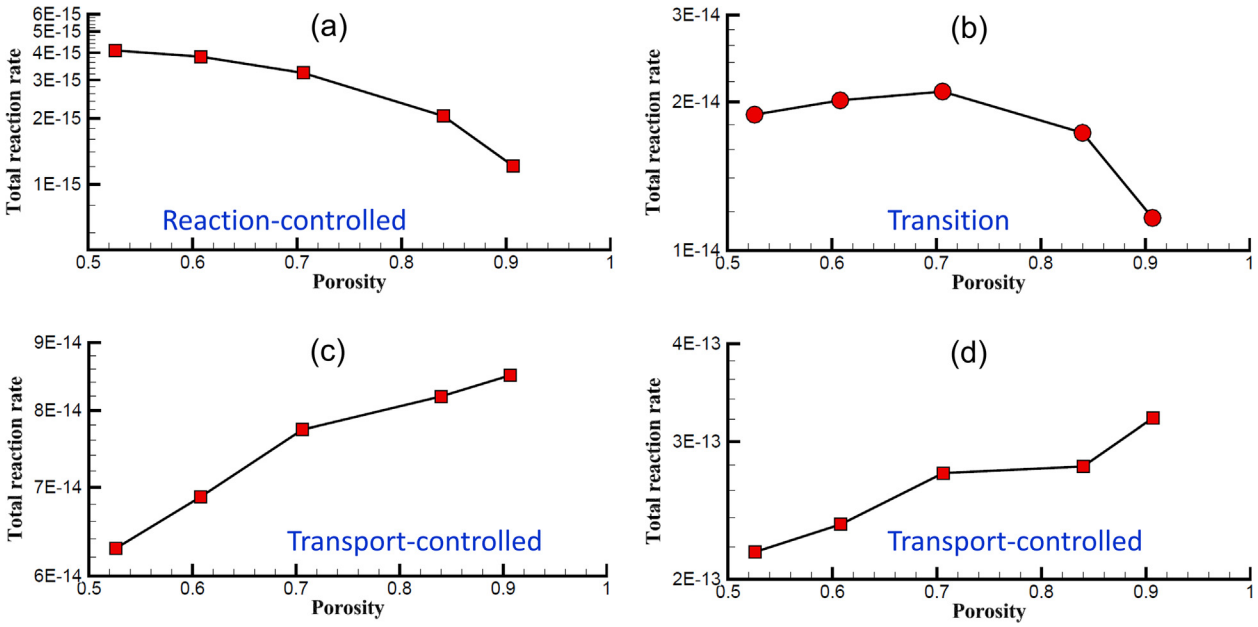

Fig. 7. Variations of the total reaction rate of different porous structures under different reaction rate constant (a) $k = 1.0 \times 10^{-7}$, (b) $k = 1.0 \times 10^{-6}$, (c) $k = 1.0 \times 10^{-5}$ and (d) $k = 1.0 \times 10^{-4}$.

layer should be sufficiently porous to ensure effective reactant gas delivery but not so much that the electron and proton conductivities are compromised. Therefore, in this section, porous media with moderate porosity of about 0.65 are studied. As shown in Fig. 8(a), macropores are distributed inside the porous catalyst layer, with the side length gradually increasing from 30 lattices (near the inlet) to 66 lattices (near the outlet), with an interval of 4 lattices between adjacent columns. Shown in Fig. 8(b) is a structure with uniform size of macropores as 48 lattices, where the total area of macropores is the same as that of in Fig. 8(a). By reversing the distribution of these macropores along x direction in Fig. 8(a), structures in Fig. 8(c) are obtained, where the size of macropores gradually decreases from the inlet to the outlet. Therefore, structures in Fig. 8(a) is a front-tight, back-loose (FTBL) structure, while that in Fig. 8(c) is a front-loose, back-tight (FLBT) structure. The structure in Fig. 8(b) is named uniform distribution (UD).

The reaction rate constant in Fig. 8 is $k = 1.01 \times 10^{-5}$. It is clearly observed from Fig. 8(a–c) that mass transport in the FLBT structure is the strongest, followed by the UD structure and finally the FTBL structure. The averaged reaction rate $< kC >$ for the FTBL, FLBT, UD as well as the original structures without macropores are listed in Table 1. First, it is expected that by adding macropores mass transport inside the porous media will be improved, and thus $< kC >$ for all the three cases with macropores are higher than the original structure, as listed in Table 1. Second, it is interesting to find out that $< kC >$ of FLBT is the highest, followed by UD, and finally FTBL. At a relatively low reaction rate constant ($k = 1 \times 10^{-7}$), the difference of $< kC >$ between FLBT, FTBL and UD is negligible; However, for a relatively high k, for example $k = 1 \times 10^{-5}$, $< kC >$ of FLBT is 18% higher than FTBL, and 11.7% higher than UD, indicating that FLBT distribution of macropores in porous media is preferred for enhancing mass transport, while the FTBL one is not desirable.

To better understand and illustrate this point, Fig. 9 shows the distribution of averaged reactant concentration along x direction. It can be seen that compared with the original case, the mass transport for FTBL case is not much increased near the left inlet, but becomes gradually stronger as x increases, in agreement with its structure characteristics. By arranging macropores near the inlet, such as that in FLBT structure, the mass transport is greatly enhanced as shown in Fig. 9, leading to more reactant supplied into the porous media and much deeper penetration of the reactant into the domain. Therefore, from the view point of enhancing mass transport, the FLBT structure is desirable.The total reaction rate $\psi = \sum kC$ is further calculated. For the original structure in Fig. 2, the number of reaction sites is 41508. For FTBL, UD and FLBT studied here, the total number of the reaction sites is 33841, 34,599 and 33561, respectively. The small discrepancy of the total number between the three hierarchical structures is because local nanoporous structures of the porous media studied in the present study are not exactly the same. The total reaction rate ψ is listed in Table 1. First, under a lower reaction rate constant, mass transport is sufficient and the negative effect of reducing reactive sites is dominant in the reactive transport process, explained in Section 4.2. Therefore, adding macropores does not help to increase ψ, and ψ of all the three cases with macropores are lower than the original case, with the one with the lowest reactive sites performing the worst which is the FTBL structure. As k increases, the positive effect of adding macropores of enhancing mass transport starts to play the role, and all the three cases with macropores have higher values of ψ than the original case. Despite the least number of reactive sites, the FLBT structure has the highest ψ because of its strong mass transport capacity. It can be found that compared with the original structure, FLBT structure leads to 20.2% increase of the total reaction rate, while the solid volume is only 73% of the original structure, causing a 26.2% reduce of the catalyst amount.

Finally, the catalyst utilization is evaluated. Currently, platinum, a noble metal, is commonly adopted as catalysts in PEMFCs. Improving the Pt utilization is critical for reducing the cell cost to promote the commercialization of PEMFCs. Fig. 10 shows predicted catalyst utilization as a function of reaction rate constant for different macropores distributions. Here, for a reactive site, if the reactant concentration on its surface is higher than 5% of the inlet concentration, then this reactive site is considered available to the reactant and catalyst there utilized. The ratio between the number of utilized reactive sites and the total reactive sites is the utilization factor η. A utilization factor of unity means that reactant reaches all reactive sites within the porous media. On the other hand, a utilization factor η approaching zero indicates high mass transport resistance, limiting access to reactive sites inside the porous media. As shown in Fig. 10, under a low reaction rate constant $k = 1 \times 10^{-7}$, since the mass transport is sufficient strong compared with the chemical reaction, η approaches unity for all the cases. As the reaction rate constant increases, η for the original structure without macropores quickly drops, indicating a considerable waste of

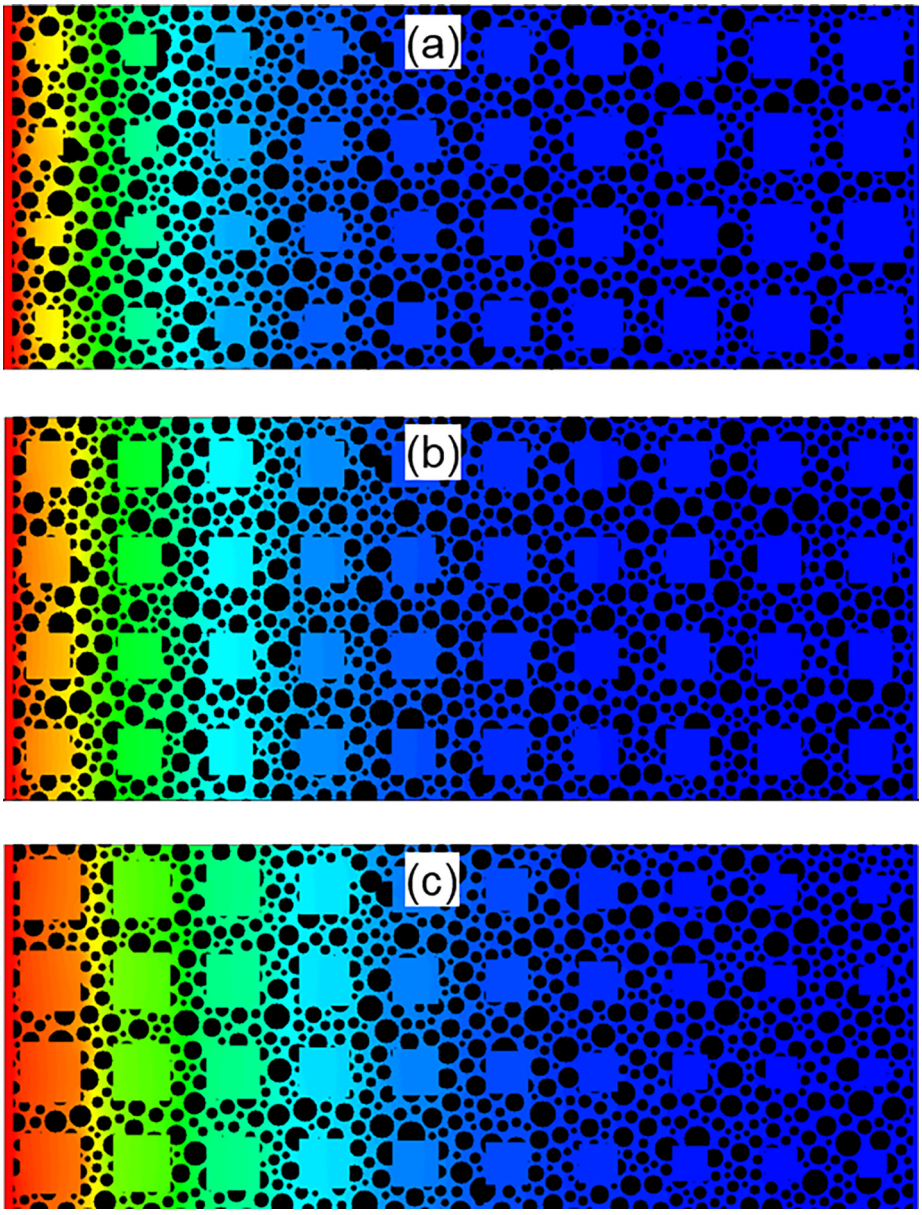

Fig. 8. Concentration distributions in porous media (a) hierarchical structure with the size of the macropores gradually increasing from the left inlet, (b) hierarchical structure with uniform size of the macropores, and (c) hierarchical structure with the size of the macropores gradually decreasing from the left inlet.

Table 1
Averaged and total reaction rate for different porous structures.

Reaction rate constant	1×10^{-7}	1×10^{-6}	1×10^{-5}	1×10^{-4}	1×10^{-3}
Original, $\langle kC \rangle$	1.29E−6	5.93E−6	1.98E−5	6.82E−5	2.49E−4
FTBL, $\langle kC \rangle$	1.37E−6	7.57E−6	2.57E−5	8.74E−5	3.08E−4
FLBT, $\langle kC \rangle$	1.40E−6	8.33E−6	3.04E−5	1.09E−4	3.72E−4
UD, $\langle kC \rangle$	1.38E−6	7.82E−6	2.72E−5	9.32E−5	3.13E−4
Original, $\sum kC$	5.35E−2	2.46E−1	8.22E−1	2.83	1.03E+1
FTBL, $\sum kC$	4.64E−2	2.56E−1	8.69E−1	2.96	1.04E+1
FLBT, $\sum kC$	4.71E−2	2.80E−1	1.02	3.64	1.25E+1
UD, $\sum kC$	4.78E−2	2.70E−1	9.42E−1	3.22	1.08E+1

the catalysts. The three structures with macropores show improved utilization of the catalyst, and again the FLBT structure shows the highest η especially under a relatively high reaction rate constant. The difference of η among different structures, however, reduces as reaction rate constant is extremely high ($k = 1 \times 10^{-3}$). This is because only catalysts very close to the left inlet are utilized in this case, and thus macropores within the porous media cannot play their roles.

On the whole, adding macropores not only reduces the catalyst loading by reducing the solid volume fraction, and hence reduces the cost, but also enhances mass transport inside the porous structures, resulting in higher catalyst utilization. As a result, fabricating macropores with porous media, especially hierarchically gradient porous media with gradually decreasing porosity along the transport direction, leads to multiple benefits, including enhanced mass transport, a lower catalyst loading and a higher catalyst utilization, all of which are desirable for catalyst application.

The above findings from pore-scale simulations have potential applications in enhancing performance of catalysts. Take catalyst layer (CL) in PEMFC as an example. The CL, sandwiched between gas diffusion layer (GDL) and proton exchange membrane (PEM), is a key component of PEMFC in which electrochemical reactions take place. The CL is a 10 μm or about thick composite porous medium containing Pt, carbon support, electrolyte and pores. Transport limitations in

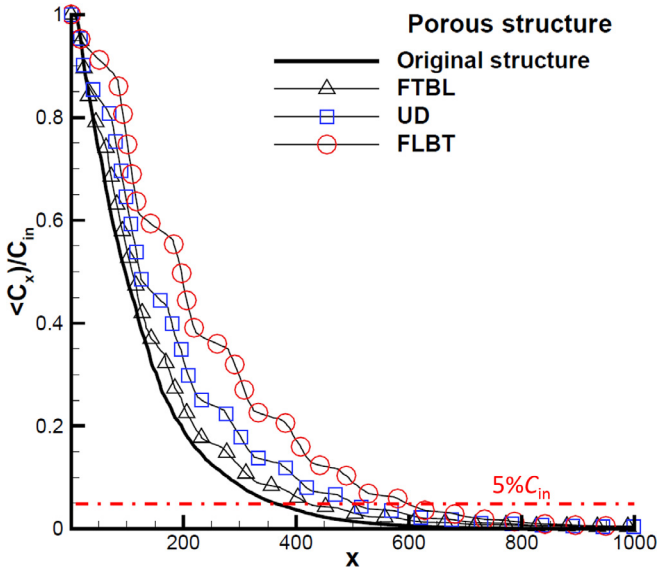

Fig. 9. The distribution of averaged reactant concentration along *x* direction in hierarchical gradient porous structures.

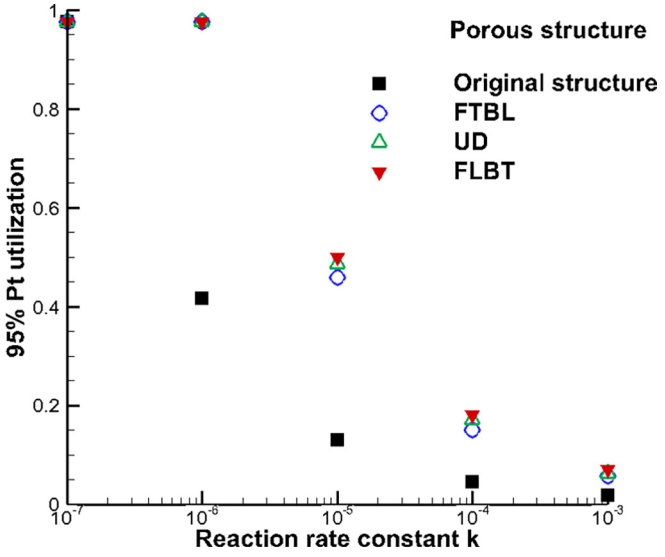

Fig. 10. Catalyst utilization as a function of reaction rate constant for different porous structures.

cathode CL of PEMFCs lead to major voltage loss. It has been found both experimentally and numerically that mass transport in the CL can be greatly improved by properly designing CL and its components (electrolyte, carbon support and Pt). While most of the studies deal with CL with a uniform structure and composition, recently there have been a few attempts to fabricate a multi-layer structure of CL [42–47]. Wang et al. [42] numerically found that a three-layer CL with higher porosity close to the GDL (obtained by adjusting Nafion content in each layer) can enhance cell performance. The above numerical results were later supported by experiments of Xie et al. [43]. Employing a lower Nafion content [43], a lower Pt loading [44,46], or both in the sub-layer [45] close to the GDL can result in lower porosity in the corresponding sub-layer, thus enhancing mass transport and cell performance.

Even through the above experimental results reported great potential, the optimal structures for the best performance of CL are not proposed. As pointed by Su et al. [46], only slightly higher performance or sometimes worse performance than uniform CL structure were generated by multi-layer CLs. For example, the three-layer CL proposed by Wang et al. [42] only causes 3% higher voltage than uniform CL at 0.8 A/cm^2. Recently, Su et al. [46] carefully investigated effects of the thickness, Nafion content and Pt loading in each sub-layer of a dual-layer CL. The best dual-layer CL structure they fabricated, which contains 23 wt% and 0.04 mg/cm^2 Pt loading in the sub-layer close to the GDL, and 33 wt% Nafion and 0.16 mg/cm^2 in the sub-layer close to the PEM, can enhance the cell performance by 35.9% compared with the single layer CL [46]. Very recently, Chen et al. [48] fabricated dual-layer CL with different Pt/C ratio and Nafion content. The best dual-layer CL structure can lead to 28.4% and 135.7% higher power density than single layer CL under high and low humidity, respectively. The FLBT hierarchical structure obtained from our pore-scale simulations can generate 20.2% increase of the total reaction rate with 26.2 reduce of the catalyst amount. The catalyst utilization is also significantly improved as can be seen from Fig. 9. The above experimental results as well as pore-scale results in the present study show that there is still much room for enhancing mass transport and improving cell performance by delicately designing the microscopic structures and compositions of CL. Pore-scale modeling is a powerful tool for this purpose which accounts for the realistic porous structures. Particularly, the present pore-scale results indicate that combining hierarchical porous structures with porosity gradient inside the CL can further enhance the reactive transport processes.

5. Conclusion

Reactive transport in porous media is widely encountered in scientific and engineering problems. Besides increasing reactive sites, enhancing mass transport is also of great importance for improving performance of the porous media. Porous structures with micropores and small mesopores have sufficient high surface area for loading reactive sites, but the transport resistance in such porous structures is high. Hierarchical porous media with combination of pores at different scales (macro, meso and micropores) provide not only sufficient surface area by micropores and small mesopores but also efficient mass transport through large mesopores and macropores. In this study, pore-scale reactive transport processes in hierarchical porous media with mesopores and macropores are studied using a LB pore-scale model. 2D original porous media with relatively low porosities yet sufficient distance between solid particles are generated. Hierarchical porous structures are further generated by adding macropores inside the original porous media. Complex interactions between porous structures and diffusion-reaction processes are revealed under different reactive transport conditions.

It is found that adding macropores can greatly enhance the mass transport and increase the penetration length of reactants. The change trend of total reaction rate is complex due to competition between two opposite effects of adding macropores, with positive one as mass transport enhancement and negative one as reactive surface reduction. Under relatively low reaction rate constant, mass transport is sufficiently strong, and thus the original porous medium without adding macropores performs the best. Under relatively high reaction rate constant, enhancing mass transport is highly required and thus hierarchical porous structures are desirable. Under a moderate reaction rate constant, the total reaction rate first increases and then drops as size of macropores in the porous medium increases.

Effects of gradient distribution of macropores within the porous medium are also investigated. A front-loose, back-tight (FLBT) structure is adopted in which side length of macropores gradually decreases from the inlet to the outlet, and front-tight, back-loose (FTBL) structure is also studied in which side length of macropores gradually increases from the inlet to the outlet. Simulation results show that FLBT distribution of macropores is preferred for enhancing mass transport and for increasing total reaction rate, while the FTBL one is not desirable. Catalyst utilization of different porous structures is also evaluated and it also reveals that the FLBT structure leads to highest catalyst utilization.

Therefore, fabricating macropores with porous media, especially hierarchically gradient porous media with gradually decreasing porosity along the transport direction (the FLBT structure), leads to multiple benefits, including enhanced mass transport, a lower catalyst loading and a higher catalyst utilization, all of which are desirable for catalyst application.

Note that only 2D studies are conducted in the present study. We have to admit that a 2D model cannot capture all the physics. However, such 2D studies often reveal the most important/fundamental mechanisms as demonstrated in the present study, and can provide insight/guidance for full 3D investigation. Numerical simulations adopting 3D realistic porous structures of electrodes in PEMFC are undertaken by the author's group.

Acknowledgements

Li Chen thanks the support of National key research and development program (2017YFB0102702) and National Nature Science Foundation of China (51776159). Qinjun Kang acknowledges the support of LANL's LDRD Program and Institutional Computing Program.

References

[1] G. Wu, K.L. More, C.M. Johnston, P. Zelenay, High-performance electrocatalysts for oxygen reduction derived from polyaniline, iron, and cobalt, Science 332 (2011) 443–447.
[2] L. Carrette, K.A. Friedrich, U. Stimming, Fuel cells – fundamentals and applications, Fuel Cells 1 (2001) 5–39.
[3] M. Skyllas-Kazacos, M.H. Chakrabarti, S.A. Hajimolana, F.S. Mjalli, M. Saleem, Progress in flow battery research and development, J. Electrochem. Soc. 158 (2011) R55–R79.
[4] W. Wang, Q. Luo, B. Li, X. Wei, L. Li, Z. Yang, Recent progress in redox flow battery research and development, Adv. Funct. Mater. 23 (2013) 970–986.
[5] D. Aydin, S.P. Casey, S. Riffat, The latest advancements on thermochemical heat storage systems, Renewable Sustainable Energy Rev. 41 (2015) 356–367.
[6] P. Pardo, A. Deydier, Z. Anxionnaz-Minvielle, S. Rougé, M. Cabassud, P. Cognet, A review on high temperature thermochemical heat energy storage, Renewable Sustainable Energy Rev. 32 (2014) 591–610.
[7] T. Soboleva, X. Zhao, K. Malek, Z. Xie, T. Navessin, S. Holdcroft, On the micro-meso-, and macroporous structures of polymer electrolyte membrane fuel cell catalyst layers, ACS Appl. Mater. Interfaces 2 (2010) 375–384.
[8] A.Z. Weber, R.L. Borup, R.M. Darling, P.K. Das, T.J. Dursch, W. Gu, D. Harvey, A. Kusoglu, S. Litster, M.M. Mench, R. Mukundan, J.P. Owejan, J.G. Pharoah, M. Secanell, I.V. Zenyuk, A critical review of modeling transport phenomena in polymer-electrolyte fuel cells, J. Electrochem. Soc. 161 (2014) F1254–F1299.
[9] K.J. Lange, P.-C. Sui, N. Djilali, Pore scale simulation of transport and electrochemical reactions in reconstructed PEMFC catalyst layers, J. Electrochem. Soc. 157 (2010) B1434–B1442.
[10] Z.-Y. Yuan, B.-L. Su, Insights into hierarchically meso–macroporous structured materials, J. Mater. Chem. 16 (2006) 663–677.
[11] J. Rouquerol, D. Avnir, C.W. Fairbridge, D.H. Everett, J.H. Haynes, N. Pernicone, J.D.F. Sing, K.K. Unger, Recommendations for the characterization of porous solids, Pure Appl. Chem. 66 (1994) 1739–1758.
[12] B. Fang, J.H. Kim, M. Kim, J.-S. Yu, Ordered hierarchical nanostructured carbon as a highly efficient cathode catalyst support in proton exchange membrane fuel cell, Chem. Mater. 21 (2009) 789–796.
[13] S. Song, Y. Liang, Z. Li, Y. Wang, R. Fu, D. Wu, P. Tsiakaras, Effect of pore morphology of mesoporous carbons on the electrocatalytic activity of Pt nanoparticles for fuel cell reactions, Appl. Catal. B 98 (2010) 132–137.
[14] E. Proietti, F. Jaouen, M. Lefèvre, N. Larouche, J. Tian, J. Herranz, J.-P. Dodelet, Iron-based cathode catalyst with enhanced power density in polymer electrolyte membrane fuel cells, Nat. Commun. 2 (2011) 416.
[15] H.-W. Liang, X. Zhuang, S. Brüller, X. Feng, K. Müllen, Hierarchically porous carbons with optimized nitrogen doping as highly active electrocatalysts for oxygen reduction, Nat. Commun. 5 (2014) 4973.
[16] P. Trogadas, V. Ramani, P. Strasser, T.F. Fuller, M.-O. Coppens, Hierarchically structured nanomaterials for electrochemical energy conversion, Angew. Chem. Int. Ed. 55 (2016) 122–148.
[17] W. Li, J. Liu, D. Zhao, Mesoporous materials for energy conversion and storage devices, Nat. Rev. Mater. 1 (2016) 16023.
[18] Y. Li, Z.-Y. Fu, B.-L. Su, Hierarchically structured porous materials for energy conversion and storage, Adv. Funct. Mater. 22 (2012) 4634–4667.
[19] M.J. Blunt, Flow in porous media — pore-network models and multiphase flow, Curr. Opin. Colloid Interface Sci. 6 (2001) 197–207.
[20] S.Y. Chen, G.D. Doolen, Lattice Boltzmann methode for fluid flows, Annu. Rev. Fluid Mech. 30 (1998) 329–364.
[21] L. Chen, Q. Kang, Y. Mu, Y.-L. He, W.-Q. Tao, A critical review of the pseudopotential multiphase lattice Boltzmann model: methods and applications, Int. J. Heat Mass Transfer 76 (2014) 210–236.
[22] G.R. Molaeimanesh, H. Saeidi Googarchin, A. Qasemian Moqaddam, Lattice Boltzmann simulation of proton exchange membrane fuel cells – a review on opportunities and challenges, Int. J. Hydrogen Energy 41 (2016) 22221–22245.
[23] M. Liu, P. Mostaghimi, High-resolution pore-scale simulation of dissolution in porous media, Chem. Eng. Sci. 161 (2017) 360–369.
[24] Th. Zeiser, P. Lammers, E. Klemm, Y.W. Li, J. Bernsdorf, G. Brenner, CFD-calculation of flow, dispersion and reaction in a catalyst filled tube by the lattice Boltzmann method, Chem. Eng. Sci. 56 (2001) 1697–1704.
[25] S.P. Sullivan, F.M. Sani, M.L. Johns, L.F. Gladden, Simulation of packed bed reactors using lattice Boltzmann methods, Chem. Eng. Sci. 60 (2005) 3405–3418.
[26] Q. Kang, P.C. Lichtner, D. Zhang, Lattice Boltzmann pore-scale model for multicomponent reactive transport in porous media, J. Geophys. Res.: Solid Earth 111 (2006) n/a-n/a.
[27] A.S. Joshi, K.N. Grew, A.A. Peracchio, W.K.S. Chiu, Lattice Boltzmann modeling of 2D gas transport in a solid oxide fuel cell anode, J. Power Sources 164 (2007) 631–638.
[28] Y. Suzue, N. Shikazono, N. Kasagi, Micro modeling of solid oxide fuel cell anode based on stochastic reconstruction, J. Power Sources 184 (2008) 52–59.
[29] J.-M. Vanson, F.-X. Coudert, M. Klotz, A. Boutin, Kinetic accessibility of porous material adsorption sites studied through the lattice Boltzmann method, Langmuir 33 (2017) 1405–1411.
[30] Z. Tian, J. Wang, Lattice Boltzmann simulation of dissolution-induced changes in permeability and porosity in 3D CO_2 reactive transport, J. Hydrol. 557 (2018) 276–290.
[31] Z. Tian, J. Wang, Lattice Boltzmann simulation of CO_2 reactive transport in network fractured media, Water Resour. Res. 53 (2017) 7366–7381.
[32] P.P. Mukherjee, C.-Y. Wang, Q. Kang, Mesoscopic modeling of two-phase behavior and flooding phenomena in polymer electrolyte fuel cells, Electrochim. Acta 54 (2009) 6861–6875.
[33] L. Chen, H.-B. Luan, Y.-L. He, W.-Q. Tao, Pore-scale flow and mass transport in gas diffusion layer of proton exchange membrane fuel cell with interdigitated flow fields, Int. J. Therm. Sci. 51 (2012) 132–144.
[34] G.R. Molaeimanesh, M.H. Akbari, A three-dimensional pore-scale model of the cathode electrode in polymer-electrolyte membrane fuel cell by lattice Boltzmann method, J. Power Sources 258 (2014) 89–97.
[35] L. Chen, Y.-L. He, Q. Kang, W.-Q. Tao, Coupled numerical approach combining finite volume and lattice Boltzmann methods for multi-scale multi-physicochemical processes, J. Comput. Phys. 255 (2013) 83–105.
[36] J.F. Delerue, E. Perrier, Z.Y. Yu, B. Velde, New algorithms in 3D image analysis and their application to the measurement of a spatialized pore size distribution in soils, Phys. Chem. Earth Part A 24 (1999) 639–644.
[37] T. Mashio, H. Iden, A. Ohma, T. Tokumasu, Modeling of local gas transport in catalyst layers of PEM fuel cells, J. Electroanal. Chem. 790 (2017) 27–39.
[38] L. Chen, Q. Kang, B.A. Robinson, Y.-L. He, W.-Q. Tao, Pore-scale modeling of multiphase reactive transport with phase transitions and dissolution-precipitation processes in closed systems, Phys. Rev. E 87 (2013) 043306.
[39] Q. Kang, P.C. Lichtner, D. Zhang, An improved lattice Boltzmann model for multicomponent reactive transport in porous media at the pore scale, Water Resour. Res. 43 (2007) W12S14.
[40] L. Chen, Q. Kang, R. Pawar, Y.-L. He, W.-Q. Tao, Pore-scale prediction of transport properties in reconstructed nanostructures of organic matter in shales, Fuel 158 (2015) 650–658.
[41] M.A. Sadeghi, M. Aghighi, J. Barralet, J.T. Gostick, Pore network modeling of reaction-diffusion in hierarchical porous particles: the effects of microstructure, Chem. Eng. J. 330 (2017) 1002–1011.
[42] Q. Wang, M. Eikerling, D.S.Z. Liu, T. Navessin, Z. Xie, S. Holdcroft, Functionally graded cathode catalyst layers for polymer electrolyte fuel cell, J. Electrochem. Soc. 151 (2004) A950–A957.
[43] Z. Xie, T. Navessin, K. Shi, R. Chow, Q. Wang, D. Song, B. Andreaus, M. Eikerling, Z. Liu, S. Holdcroft, Functionally graded cathode catalyst layers for polymer electrolyte fuel cells II. experimental study of the effect of nafion distribution, J. Electrochem. Soc. 152 (2005) A1171–A1179.
[44] A.D. Taylor, E.Y. Kim, V.P. Humes, J. Kizuka, L.T. Thompson, Inkjet printing of carbon supported platinum 3-D catalyst layers for use in fuel cells, J. Power Sources 171 (2007) 101–106.
[45] K.H. Kim, H.J. Kim, K.Y. Lee, J.H. Jang, S.Y. Lee, E. Cho, I.H. Oh, T.H. Lim, Effect of Nafion® gradient in dual catalyst layer on proton exchange membrane fuel cell performance, Int. J. Hydrogen Energy 33 (2008) 2783–2789.
[46] H.-N. Su, S.-J. Liao, Y.-N. Wu, Significant improvement in cathode performance for proton exchange membrane fuel cell by a novel double catalyst layer design, J. Power Sources 195 (2010) 3477–3480.
[47] H. Su, T.-C. Jao, S. Pasupathi, B.J. Bladergroen, V. Linkov, B.G. Pollet, A novel dual catalyst layer structured gas diffusion electrode for enhanced performance of high temperature proton exchange membrane fuel cell, J. Power Sources 246 (2014) 63–67.
[48] G.-Y. Chen, C. Wang, Y.-J. Lei, J. Zhang, Z. Mao, Z.-Q. Mao, J.-W. Guo, J. Li, M. Ouyang, Gradient design of Pt/C ratio and Nafion content in cathode catalyst layer of PEMFCs, Int. J. Hydrogen Energy 42 (2017) 29960–29965.